Yang S, Baker NJ, Mecrow BC, Smith D, Atkinson G, Hilton C, Perovic DK, Kakavas I, Sooriyakumar G, Harvey P.

Magnet Losses and Demagnetisation in a Permanent Magnet In-wheel Electric Vehicle Traction Motor.

***In: IEEE International Electric Machines and Drives Conference (IEMDC)*. 2015, Idaho, USA: IEEE.**

DOI link to article:

http://dx.doi.org/10.1109/IEMDC.2015.7409313

Date deposited:

13/05/2016

Magnet Losses and Demagnetisation in a Permanent Magnet In-wheel Electric Vehicle Traction Motor

Sichao Yang, Nick J. Baker, Barrie C. Mecrow, Daniel Smith, Glynn Atkinson, Chris Hilton, Dragica K. Perovic, Ioannis Kakavas, Gunaratnam Sooriyakumar, Paul Harvey

***Abstract*--This paper investigates magnet topologies and their susceptibility to demagnetisation in an in-wheel motor for an electric vehicle. The analysed motor is a high torque density, low speed, surface-mounted permanent magnet (SMPM) modular motor with fractional slot concentrated winding (FSCW) and an outer rotor. The rich spatial stator MMF harmonics present in the air gap have two effects: they generate AC losses in the magnets and they can increase the peak demagnetising field which the magnets experience. In this work, methods are first developed to give greater insight into the magnet loss mechanisms, thereby indicating when magnet segmentation is beneficial. The methods are then extended to examine how different rotor designs are affected by both loss and demagnetisation fields, showing major differences between rotor topologies.**

***Index terms*--In-wheel motor, V shape PM, FSCW, Magnet demagnetisation, Analytical prediction, 2D FEA, eddy current, stator MMF harmonics, Current sheet, Magnet segmentation**

I. INTRODUCTION

Fractional slot, concentrated windings help machine designers to gain significant advantages in increasing the active to overall axial length ratio, fill factor, and thermal conductivity. They also ease the manufacturing and assembly process. However, in addition to the torque producing stator MMF, rich spatial harmonics are generated and can cause strong parasitic effects [1-3].

This work concentrates upon machine designs for direct drive in-wheel motors. Many prototypes have been built and extensively tested by the authors in electric vehicles. In previous papers they have discussed cost reduction [4] and fault tolerant performance [5].

The aim of this paper is to provide a magnet loss evaluation system for fractional slot, concentrated winding PM motors and understand how to minimise this loss. The paper then goes on to identify methods of reducing the peak demagnetisation field experienced by each magnet. A number of tools are adopted and developed to identify the origin of the magnet loss in the in-wheel motor.

This project is financially sponsored by Protean Electric Limited.

Authors Sichao Yang, Nick J. Baker, Barrie C. Mecrow, Daniel Smith and Glynn Atkinson are with Electric Power Research Group, Electrical Engineering School, Newcastle University, NE1 7RU, United Kingdom. (email: s.yang6@ncl.ac.uk)

Authors Chris Hilton, Dragica K. Perovic, Ioannis Kakavas, Gunaratnam Sooriyakumar and Paul Harvey are with Protean Electric Limited, Silvertree, Unit 10B, Coxbridge Business Park, Alton Road, Farnham, Surrey, GU10 5EH, United Kingdom.

II. IN-WHEEL MOTOR

The authors in [4, 5] propose the in-wheel propulsion solution for EV applications mainly due to its essential merit - integration. By integrating the drive package into the wheels, it frees up the packaging space on the vehicle platform, permitting additional energy storage components or simply more passenger space [6].

The high efficiency target [7] inspired the designer to link the motor to the drive train by using an outer rotor arrangement to attach the motor package onto the wheel. It prohibits any mechanical gear transmission but also imposes a restricted shape and space for the machine designer. The permanent magnet synchronous machine in Figure 1 was chosen due to its high efficiency and torque density.

Limited by standard car wheel size, the ratio of overall axial length to outside diameter is only 0.15. This necessitates the use of high pole numbers and concentrated windings in order to have a very short end winding length. A 64 pole, 72 slot, machine was chosen: the high pole number also results in small core back depths, whilst the modest peak speed means that excessive electrical frequencies are avoided. The result is a ring type machine, leaving the inner space for mechanical brakes and integrated electronic converters.

The high spatial harmonic contents of the stator MMF rotate asynchronously relative to the rotor, inducing eddy currents and subsequent heat in the magnets. The heat is hard to dissipate due to no direct cooling method applied on the outer rotor. The magnet temperature is measured at 60°-80° Celsius in the motor designed in [5] at steady state. Although with the existing design there is no risk of demagnetisation, with designs in which the magnet material is reduced in order to lower cost, this is no longer the case. [4] Keeping the rotor cool makes demagnetization less likely and increases the magnet residual flux density, thereby maximising performance.

By moving from surface mounted magnets to interior magnets, arranged in a V shape, it has been found that the magnet depth can be greatly reduced without any risk of demagnetisation. There could be two possible reasons for this: either the magnet leakage flux is increased, hence increasing the operating point of the magnet, or somehow the magnet is being screened from the armature reaction flux.[8] [9]

Insight into why the interior magnet design is less susceptible to demagnetisation has been gained by examining all the spatial harmonics of the stator in turn, understanding whether they penetrate the magnets and whether they cause significant loss.

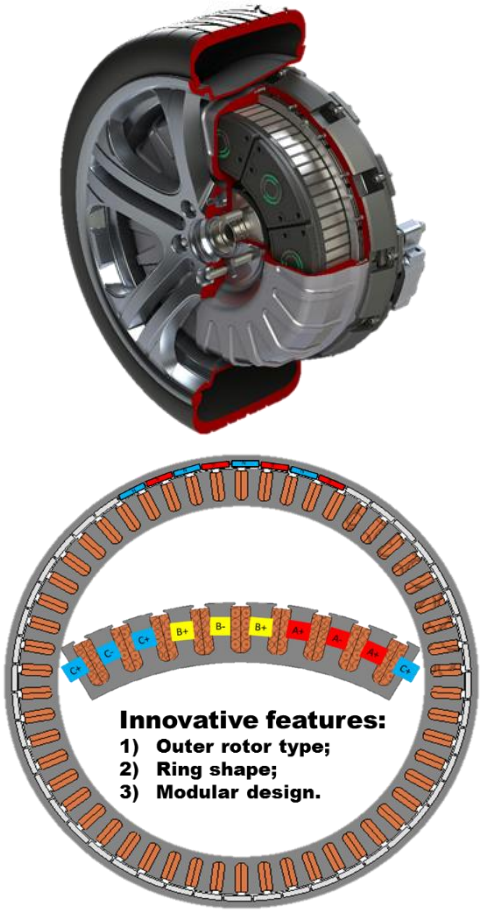

Figure 1 motor design in [4]

III. THE STATOR MMF AND RESULTING FIELD

The stator MMF produces asynchronous travelling magnetic fields of various pole numbers in the air gap. To represent it an analytical model is developed based on Fourier analysis of an idealized air-gap MMF distribution. Note that sinusoidal phase current input has been assumed: in reality PWM harmonics can cause additional loss [10]. The actual machine has 72 slots and 64 poles. The MMF pattern repeats eight times round the machine, so it is essentially eight machines, each with 9 slots and 8 poles. To simplify the subsequent discussion analysis will be performed on a 9-8 machine: all harmonics can then be multiplied by eight to find their order in the actual machine.

A. Fourier transform of stator MMF

A single energized slot of a 9 slot, 8 pole machine is illustrated in Figure 2. The sum of the magnetising field around the indicated flux path is equal to the MMF enclosed, as described in equations (1) and (2). It is assumed that the slot MMF is dropped linearly across the slot opening, giving an even tangential magnetizing field at the slot opening and zero tangential field at the tip of the tooth.

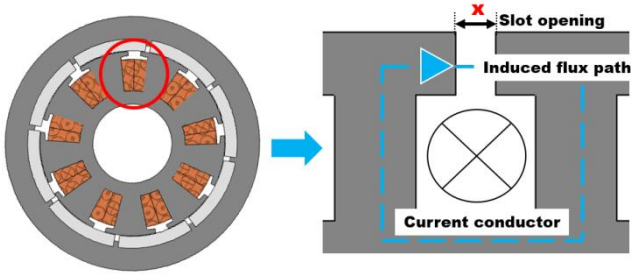

Figure 2 the single energised slot unrolled from an 8 pole, 9 slot machine

$$\oint_C H_t\, dl = \iint_S J\, dS = MMF_{slot} \quad (1)$$

$$H_{t,slot}(t) = \frac{MMF_{slot}(t)}{x} \quad (2)$$

B. Decomposition

In equation (3), it can be seen that the magnetizing field at the stator bore resulting from a single energized slot is decomposed into its Fourier components of different pole numbers, amplitude and direction.

$$\begin{aligned} H_t(\theta,t) &= \frac{H_t(t)(\theta_b-\theta_a)}{2\pi} + \\ &\sum_{n=1}^{\infty}\frac{H_t(t)}{n\pi}[(\sin n\theta_b - \sin n\theta_a)\cos n\theta + \\ &(\cos n\theta_a - \cos n\theta_b)\sin n\theta] = \frac{H_t(t)(\theta_b-\theta_a)}{2\pi} + \\ &\sum_{n=1}^{\infty}\left[\sin\left(n\frac{(\theta_b-\theta_a)}{2}\right)\cos(n(\frac{(\theta_b+\theta_a)}{2}-\theta))\right]\frac{H_t(t)}{n\pi} \end{aligned} \quad (3)$$

Where θ_a and θ_b are the angle between the slot opening.

Similarly, the full air gap magnetic field in equation (5) is the summation of the field due to each slot, defined at different locations in equation (4).

$$\theta_{a,b}(m) = \theta_{a,b} + (m-1)\lambda_{stator} \quad (4)$$

$$\begin{aligned} H_t(\theta,t) = \sum_{n=1}^{\infty}\sum_{m=1}^{slot\ no}\frac{H_t(t)}{n\pi}[(\sin n\theta_b(m) - \\ \sin n\theta_a(m))\cos n\theta + (\cos n\theta_a(m) - \\ \cos n\theta_b(m))\sin n\theta] \end{aligned} \quad (5)$$

Where λ_{stator} is the stator slot pitch in mechanical degrees; m is the slot number; n is harmonic frequency order equating to the pole pair of the air gap field.

The stator surface H field and its Fourier components are shown in Figure 3 and Figure 4. Figure 5 is a graphical demonstration of the first three harmonics in the air gap. For this 8 pole, 9 slot machine the asynchronous 2 pole and 10 pole fields are rotating opposite to the 8 pole torque producing field.

Throughout the rest of this paper the torque producing field will be referred to as the 4th harmonic. This is an 8 pole field in the 8 pole machine and a 64 pole field in the full 64 pole machine. The 2 pole, sub synchronous field will be regarded as the first harmonic. This becomes a 16 pole field in the 64 pole machine. Finally there is a large backwards rotating 10 pole field in the 8 pole machine, corresponding to an 80 pole field in the 64 pole machine. This will be referred to the 5th harmonic as it is five times the lowest pole number field present.

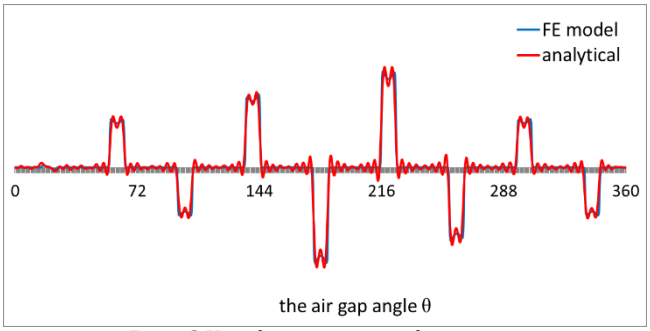

Figure 3 H_t in the air gap at a random time instant

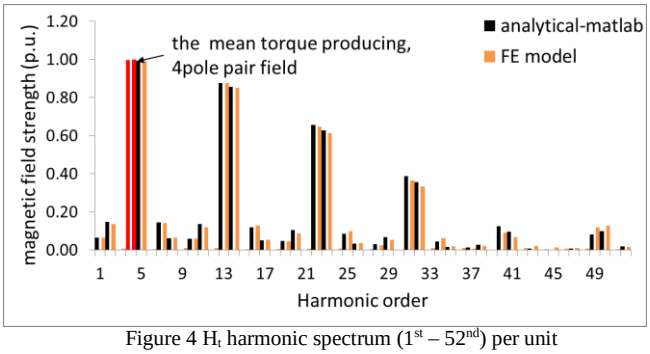

Figure 4 H_t harmonic spectrum (1^{st} – 52^{nd}) per unit

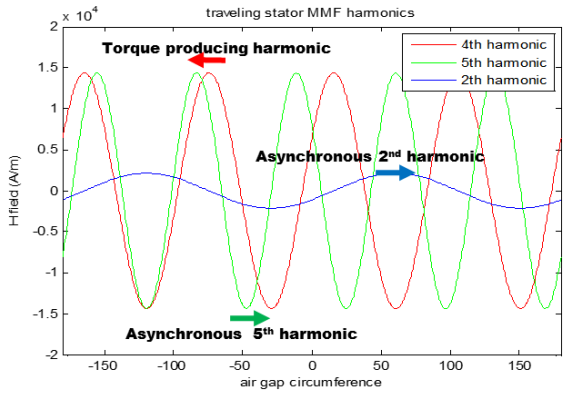

Figure 5 the 2^{nd}, 4^{th} and 5^{th} harmonic rotating direction demonstration

IV. LOSS CALCULATION

With the magnetic field defined, the loss can be calculated in different ways:

1) 2D analytical calculation based on the full definition of the magnetic potential in the full air gap region, as in [11-13].
2) 2D analytical loss indication for different cases defined by harmonic wavelength to magnet width ratio [14].
3) 2D FE analysis based on the current sheet representation of the travelling magnetic field from the stator side.

The approach in 1) can give an accurate prediction of the surface mounted magnet loss, when compared to 2D FEA, if the reaction field of the induced eddy currents and the magnetic circuit saturation can be ignored. However, it is not suited to interior magnet topologies. Method 2) can generate a rapid magnet loss index for initial comparison, however no direct magnet loss can be calculated and the skin effect is not considered. [15]. Therefore, method 3) is developed in this work without concerning computationally expensive 3D approach [16].

A. *Current sheet in FE software*

For each harmonic a rotary current sheet is created: for example the 10 pole, backward rotating, 5^{th} harmonic field is shown in figure 7, with the stator magnetic circuit modelled as a highly permeable material.

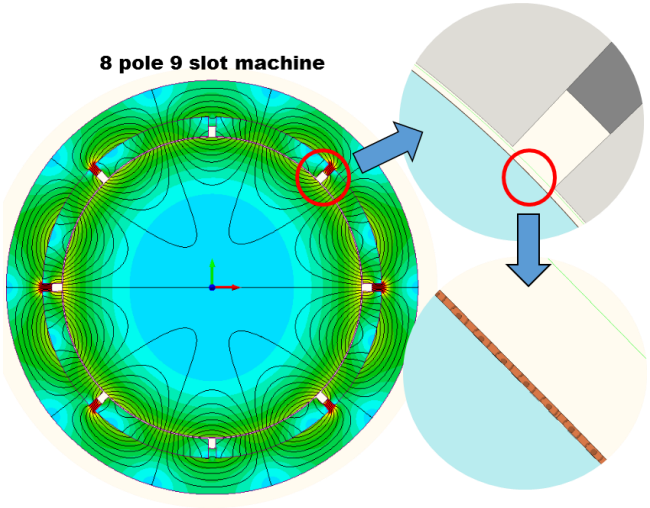

Figure 6 the rotary current sheet in 10 pole harmonic

B. *The overall and single harmonic loss*

To calculate the magnet loss, the traveling harmonic field is generated first by re-composing all the harmonics up to the 52nd (this range is chosen to balance the computational time and result accuracy). This source field determines the total current sheet, which is used to solve the 2D transient FEA model.

The losses from the current sheet model and the model with a complete stator are compared in Figure 7. Satisfactory accuracy has been achieved using the current sheet model, validating the approach. Furthermore, it is predicted that 85% of the loss is eliminated when the negatively rotating 5th harmonic is removed.

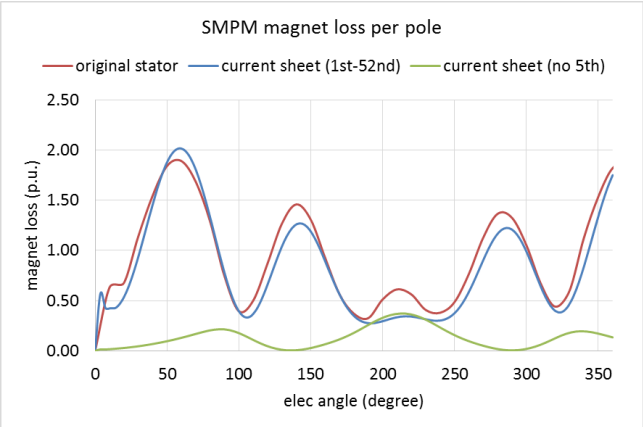

Figure 7 the magnet loss per pole per unit in 64p72s SMPM

To prove the significance of 5^{th} harmonic loss, the harmonic loss summation principle is applied: harmonics are

injected into the current sheet model individually to generate the time average harmonic loss. There is less than 5% difference between the average loss predicted by the current sheet in Figure 7 and the summed average loss produced by each harmonic in Figure 8. The 5th harmonic acting alone is predicted to contribute 87% of the total loss.

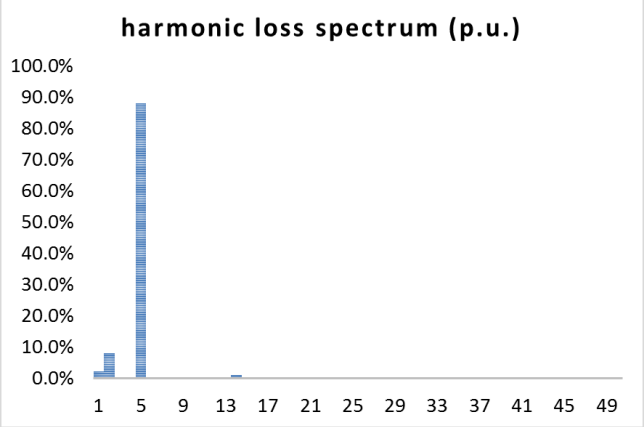

Figure 8 the harmonic loss spectrum in 64p72s SMPM

Hence, both calculations identify the 5th harmonic as the biggest loss contributor. Other contributors to loss are the 2nd harmonic, producing 8%, the 1st harmonic, 2 pole field producing 2% and the 14th harmonic producing 1% of the magnet loss. To reduce the 5th harmonic loss, segmentation options are investigated in the next section.

V. MAGNET LOSS REDUCTION

A. *The eddy current inducing mechanism*

The eddy current inducing mechanism is studied first to discover how to segment the magnet to reduce the loss.

With the current sheet created in 2D FE, the eddy current inducing mechanism for different magnetic field harmonics can be observed and classified according to the harmonic wavelength to magnet width ratio (λ_n/w) [14].

The eddy current density at any one point varies sinusoidally in response to the 5th harmonic source field. Hence the loss density at that position has a dc value and a twice frequency oscillation. Integration of the loss density across the full magnet produces the instantaneous magnet loss: the time average loss can be defined by averaging the maxima and minima of the instantaneous loss calculation.

Following the arguments used in [10] it is useful to consider the different exciting harmonics in turn. Sub-harmonics of the pole number and those near to the pole number, act differently to higher frequency harmonics, so each will be dealt with in turn.

Firstly consider the second harmonic, which produces a 32 pole field in the 64 pole machine. The maximum instantaneous loss occurs when the normal flux enters the magnet on one side of the magnet and exits it on the other side. This is illustrated in Figure 9 by applying the 2nd stator MMF harmonic in current sheet model. The minimum instantaneous loss occurs when the flux is centered over the magnet: loss is near zero with only small eddy currents formed. It is clear that this harmonic penetrates right through the magnet, so the loss density is distributed throughout its depth. As expected the majority of the loss is at the magnet circumferential edges. At the point of greatest loss the eddy currents flow in a single loop down one side of the magnet and up the other.

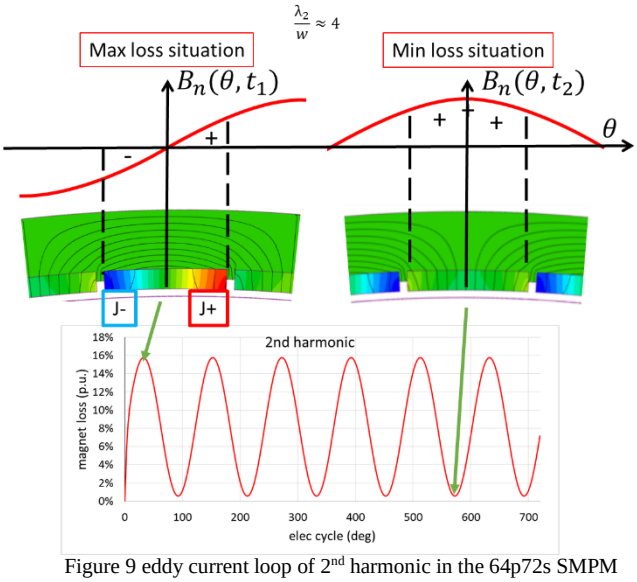

Figure 9 eddy current loop of 2nd harmonic in the 64p72s SMPM

Consider now the 5th harmonic, which produces an 80 pole field in the 64 pole machine. The maximum loss in this case also occurs at the time instant when there is zero magnetic flux at the centre of the magnet and the minimum when the harmonic is centred over the magnet, as shown in figure 11. Once more the currents flow in a single loop and the majority of the loss is at the circumferential edges of the magnet but, because the harmonic wavelength of the magnet is smaller, there is less penetration through the magnet and so the peak loss is near the surface of the magnet.

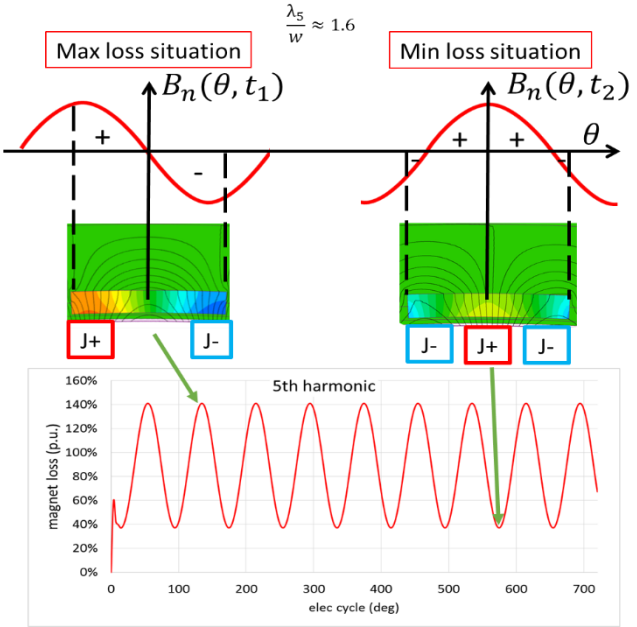

Figure 10 eddy current loop(s) of 5th harmonic in the 64p72s SMPM

Finally, consider the 14th harmonic, which is the only super-harmonic to produce significant loss. In this case the maximum loss occurs when there are three eddy current loops, with four current loops at the minimum loss time instant. Loss is distributed throughout the magnet in a circumferential sense, but is concentrated at the magnet surface because the high pole number flux does not penetrate so much through the magnet.

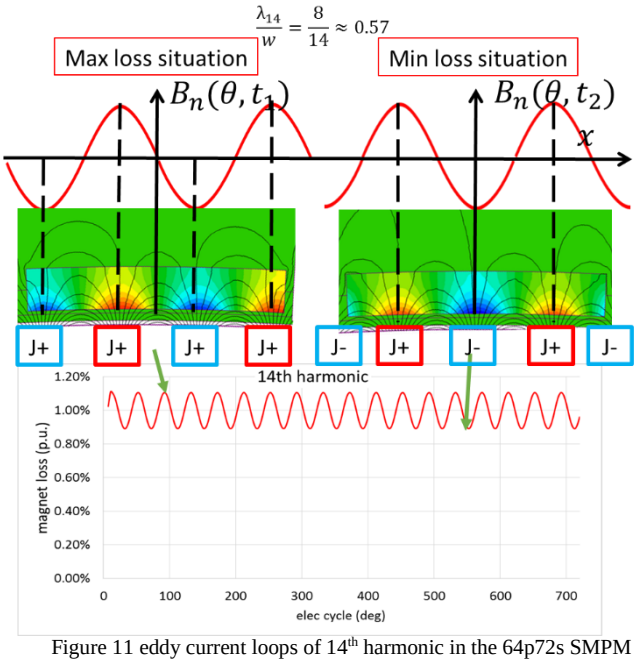

Figure 11 eddy current loops of 14th harmonic in the 64p72s SMPM

B. *Segmentation*

Circumferential segmentation is extremely useful for the sub-harmonics and harmonics near the fundamental which have small number of eddy current loops, including the main loss producing 5th harmonic and the 2nd harmonic.

When segmented into 2 pieces, the eddy currents can no longer flow in a single loop. Two loops are created, which effectively halves the peak flux linkage for any one eddy current path and so greatly reduces the resultant loss. This phenomena is illustrated in Figure 12 and 14, which show how the loss in each segment varies with time. The minimum loss point in each segment now occurs when that segment has zero net flux linking it, corresponding to the greatest rate of change of flux-linkage.

Hence, for all sub and near fundamental harmonics, segmentation of the magnet into 2 pieces per pole greatly reduces the magnet loss.

Note however that with the higher 14th harmonic, two piece segmentation will not significantly affect the eddy current distribution, because each segment is still greater than a single harmonic pole span. It means the eddy current can still form complete loop(s) with unaffected peak flux linkage. In order for segmentation to be effective it would have to be such that each segment spanned only a harmonic pole or less ($\frac{\lambda_n}{w} \geq 2$), which would require at least 4 segments per pole.

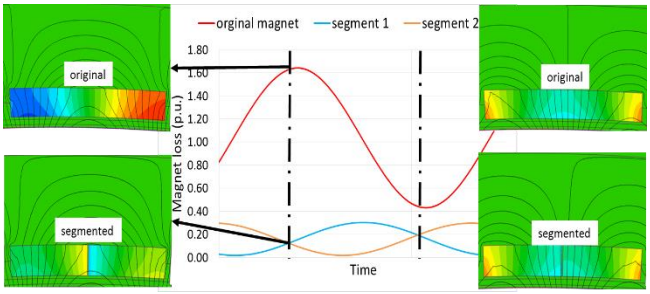

Figure 12 the circumferential segmentation effect

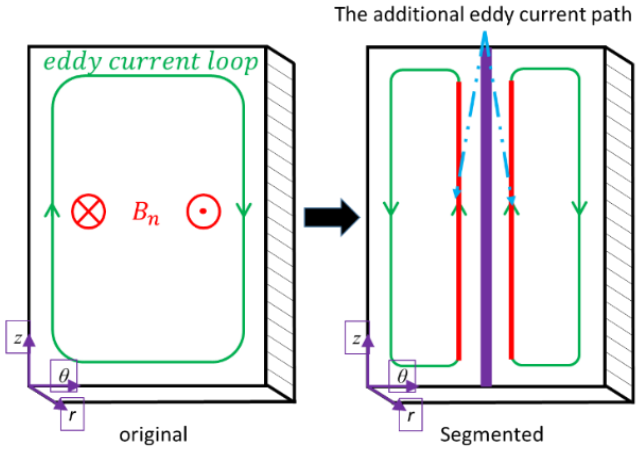

Figure 13 the additional eddy current path, hence resistance, introduced in the sub harmonics and harmonics near the fundamental

Because the 5th harmonic dominates the loss the single magnet per pole was segmented into 2 pieces. Figure 15 shows the effect upon magnet loss as a function of time. Overall loss is reduced by 65%, resulting in a cooler rotor and magnets which are less prone to demagnetisation.

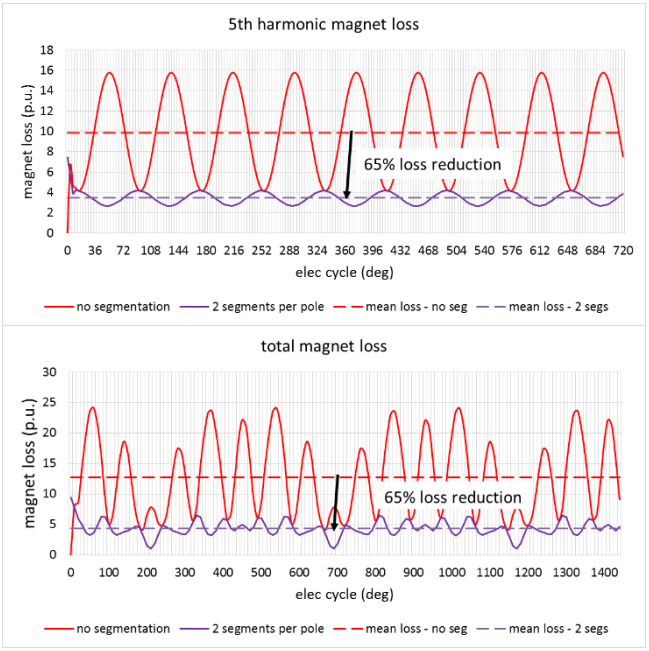

Figure 14 the magnet loss due to segmentation in a 72s64p machine

The above discussion does not include axial segmentation. Axial segmentation only works if the circumferential

eddy current path length is greater than the axial length. [14, 15]. In this machine the axial length to magnet width ratio is 3.5 [4, 5]. Therefore, by splitting each magnet into 10 axial segments the magnet loss is further reduced.

VI. Demagnetization

Segmentation reduces loss and hence temperature, which makes the magnets more resistant to demagnetization. However, it does not reduce the magnitude of the demagnetization field, which is the fundamental source of demagnetization. To reduce material cost the magnet depth can be reduced but, at peak demagnetizing current, the magnets move over the knee of the B-H curve and can be permanently demagnetized, as shown in figure 16 (a). Interestingly, the magnets of each pole do not experience the same demagnetizing field at any one instant. The peak demagnetizing field occurs at the instant that the peak 5th harmonic field coincides with the peak of the main torque producing field. The sum of these two fields occurs at the third from right magnet in figure 16 (a) at the instant of modelling.

Compare now Figure 15(b) with that of 16(a). In (b) the magnets have been changed to an interior V shape. There is the same volume of magnet and the back EMF remains virtually identical, but there is no demagnetization.

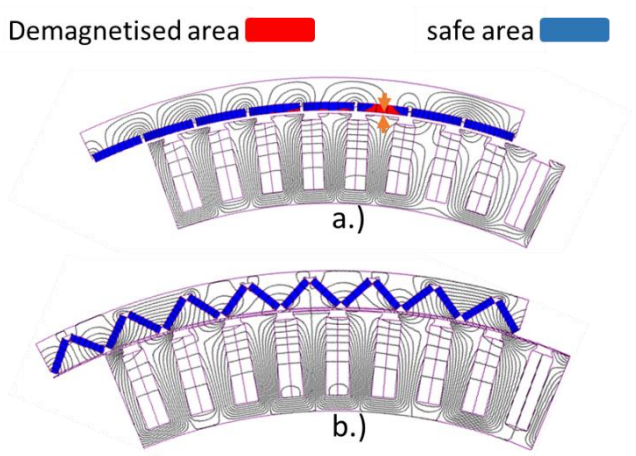

Figure 15 the demagnetisation prediction of SMPM and V models in the worst scenario described in section II (The magnet grade is: Sintered Neodymium-Iron-Boron Magnets – N45SH, the knee point at 100°C is 0.3T.) [4]

Figure 16 and Figure 18 attempt to illustrate why the V shaped magnets are much less prone to demagnetization. Figure 17 shows the magnet operating point along the magnet surface. First, in black, is the no-load operating point for each case. Both magnets operated with a flux density close to 0.8 Tesla, with the circumferential ends of the magnets having a lower flux density due to slotting effect. This drop is actually greater in the V shaped design at the bottom of the V.

In blue is the impact of the torque producing 4th harmonic, though in this case it is positioned close to the negative d-axis. Both magnets experience a significant drop in flux density, but remain safely above 0.3 Tesla, which is the point of irreversible demagnetization.

Finally, in red, is the case with all harmonics included. Most of the surface mounted magnet machine magnets are beyond the knee of the B-H curve, whilst the V shaped magnet arrangement remains safely above, apart from the very peripheral ends of the magnets. The reason for this is that all higher order harmonics are screened out by the magnet triangle above the magnet. High pole number fields enter and leave this triangle without ever linking the magnet. In the 64 pole, 72 slot machine screening of the 5th harmonic field is only partial because it is so close to the pole number, but it is still effective enough to have a significant impact.

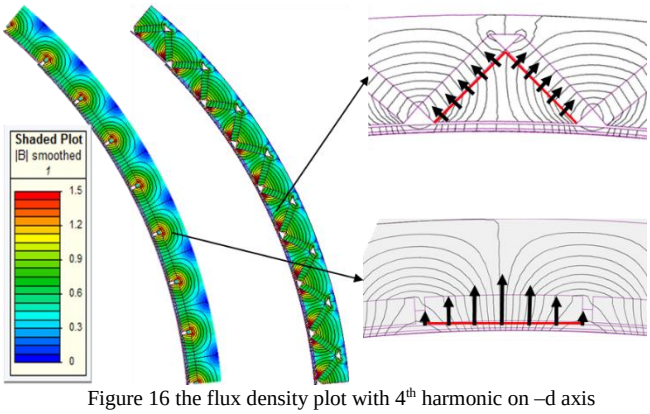

Figure 16 the flux density plot with 4th harmonic on –d axis

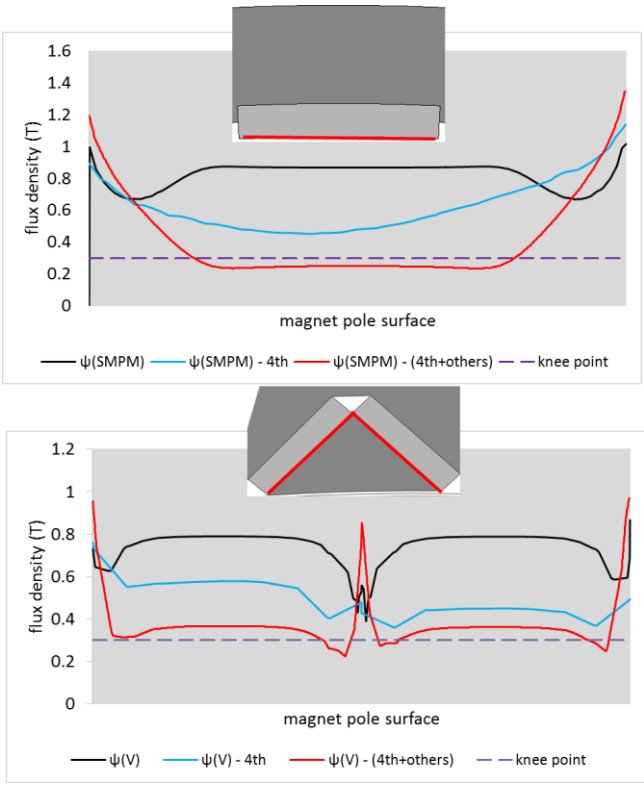

Figure 17 the flux density on the surface of the magnet(s) in SMPM and V (the black line is the flux density with only magnet energised; the blue line is when the armature flux from 4th harmonic opposing the magnet; the red is the worst scenario with all harmonics included.)

Interestingly the V shaped magnet arrangement has a further advantage over the surface mounted magnet arrangement. For the same torque target and with the same

magnet mass, less electric loading is required in the V shape PM due to the assistance of reluctance torque, which means the magnet loss can be further reduced, compared to the SMPM.

VII. CONCLUSION

Analytical and FE tools have been developed to gain a deeper insight into the magnet loss inducing mechanism in a permanent magnet in-wheel motor with 64 poles and 72 slots. The magnet loss is shown to be dominated by the presence of a negatively rotating 80 pole field, and it is shown how this loss can be reduced by 65% by segmenting the magnets into two circumferential parts. To reduce costs magnet mass reduction is desirable and it is shown how, by adopting V shaped magnets in an interior configuration, this can be achieved with reduced risk of irreversible demagnetization.

VIII. REFERENCE

[1] T. J. Juha Pyrhonen, Valeria Hrabovcova, "Design of Rotating Electrical Machines," ed, 2008, pp. 105-122.

[2] A. M. El-Refaie, "Fractional-Slot Concentrated-Windings Synchronous Permanent Magnet Machines: Opportunities and Challenges," Industrial Electronics, IEEE Transactions on, vol. 57, pp. 107-121, 2010.

[3] N. Bianchi and E. Fornasiero, "Impact of MMF Space Harmonic on Rotor Losses in Fractional-Slot Permanent-Magnet Machines," Energy Conversion, IEEE Transactions on, vol. 24, pp. 323-328, 2009.

[4] Y. Sichao, N. J. Baker, B. C. Mecrow, C. Hilton, G. Sooriyakumar, D. Kostic-Perovic, et al., "Cost reduction of a permanent magnet in-wheel electric vehicle traction motor," in Electrical Machines (ICEM), 2014 International Conference on, 2014, pp. 443-449.

[5] C. J. Ifedi, B. C. Mecrow, S. T. M. Brockway, G. S. Boast, G. J. Atkinson, and D. Kostic-Perovic, "Fault-Tolerant In-Wheel Motor Topologies for High-Performance Electric Vehicles," Industry Applications, IEEE Transactions on, vol. 49, pp. 1249-1257, 2013.

[6] P. Electric. (2011). In-wheel motor development. Available: http://www.proteanelectric.com/en/white-papers/

[7] A. T. de Almeida, F. J. T. E. Ferreira, and J. A. C. Fong, "Standards for Efficiency of Electric Motors," Industry Applications Magazine, IEEE, vol. 17, pp. 12-19, 2011.

[8] J. Blum, J. Merwerth, and H. G. Herzog, "Magnet eddy-current losses in interior permanent magnet machines with concentrated windings - analysis and reduction of the major source," in Power Electronics, Machines and Drives (PEMD 2014), 7th IET International Conference on, 2014, pp. 1-6.

[9] Z. Azar, L. J. Wu, D. Evans, and Z. Q. Zhu, "Influence of rotor configuration on iron and magnet losses of fractional-slot IPM machines," in Power Electronics, Machines and Drives (PEMD 2010), 5th IET International Conference on, 2010, pp. 1-6.

[10] K. Yamazaki and A. Abe, "Loss Investigation of Interior Permanent-Magnet Motors Considering Carrier Harmonics and Magnet Eddy Currents," Industry Applications, IEEE Transactions on, vol. 45, pp. 659-665, 2009.

[11] R. L. Stoll, The analysis of eddy currents: Clarendon Press, 1974.

[12] K. Yamazaki and Y. Fukushima, "Effect of Eddy-Current Loss Reduction by Magnet Segmentation in Synchronous Motors With Concentrated Windings," Industry Applications, IEEE Transactions on, vol. 47, pp. 779-788, 2011.

[13] F. Martin, M. E. H. Zaim, A. Tounzi, and N. Bernard, "Improved Analytical Determination of Eddy Current Losses in Surface Mounted Permanent Magnets of Synchronous Machine," Magnetics, IEEE Transactions on, vol. 50, pp. 1-9, 2014.

[14] B. Aslan, E. Semail, and J. Legranger, "General Analytical Model of Magnet Average Eddy-Current Volume Losses for Comparison of Multiphase PM Machines With Concentrated Winding," Energy Conversion, IEEE Transactions on, vol. 29, pp. 72-83, 2014.

[15] H. Wan-Ying, A. Bettayeb, R. Kaczmarek, and J. C. Vannier, "Optimization of Magnet Segmentation for Reduction of Eddy-Current Losses in Permanent Magnet Synchronous Machine," Energy Conversion, IEEE Transactions on, vol. 25, pp. 381-387, 2010.

[16] M. Mirzaei, A. Binder, B. Funieru, and M. Susic, "Analytical Calculations of Induced Eddy Currents Losses in the Magnets of Surface Mounted PM Machines With Consideration of Circumferential and Axial Segmentation Effects," Magnetics, IEEE Transactions on, vol. 48, pp. 4831-4841, 2012.

IX. BIOGRAPHIES

Sichao Yang received a Bsc in Southwest University for Nationalities, China, in 2011 and an MSc in Newcastle University, UK, in 2012. He is currently working towards the PhD degree in Newcastle University, designing high torque, fault tolerant and cost competitive in-wheel motors for Electric Vehicles, which is sponsored by Protean Electric.

Nick J. Baker is a Lecturer within Newcastle University's Electrical Power Group. He obtained a PhD from Durham University, UK, in 2003 for work in electrical machine design for marine renewable energy devices. He subsequently worked as an academic at Lancaster University (2005-2008), a renewable energy consultant at TNEI.

Barrie C. Mecrow is Professor of Electrical Power Engineering and head of the School of Electrical and Electronic Engineering at Newcastle University, UK. His research interests include fault tolerant drives, high performance PM machines and novel switched reluctance drives. He is actively involved with industry in the aerospace, automotive and consumer product sectors, who fund a large range of projects.

Daniel Smith received an MEng in Engineering, Economics and Management from Oxford University in 2008 before completing a PhD in High Speed High Power Motor Design with the successful delivery of a 1.1MW, 30,000rpm PM dynamometer. He currently works for an industrial partner embedded in Newcastle university, supervising PhD students and leading blue sky motors research.

Glynn J. Atkinson is a Lecturer within Newcastle University's Electrical Power Group. He has carried our research in fault-tolerant machines for aerospace applications, focusing on high-power, high-speed permanent magnet machines, plus -D machine topologies using soft magnetic composites with applications in the automotive and high volume manufacturing sectors.

Chris Hilton is the Chief Technology Officer at Protean Electric having previously held roles in the fields of communications electronics, satellite navigation and particle physics research. Hi holds a PhD in physics from the University of Manchester and a masters degree in mathematics from the University of Cambridge, UK.

Dragica Kostic Perovic gained her DPhil in electrical engineering at University of Sussex, UK, researching fault detection in induction motor and pump and first degree at University of Belgrade, Serbia. She is currently working as a Principal Motor Design Engineer at Protean Electric Ltd, UK, with main interests in the area of electromagnetic motor design, and DFMEA as a design process.

Ioannis Kakavas obtained his degree in Mechanical Engineering from the Aristotle University of Thessaloniki in Greece in 2010. After completing his PhD in automotive power-train efficiency at Imperial College, London, he joined the Advanced Motor Research team at Protean Electric Ltd.

Gunaratnam Sooriyakumar works for Protean Electric as a specialist in electric machines and drives. He obtained a BSc in Electrical and Electronic Engineering from the University of Peradeniya in Sri Lanka and a PhD from the University of East London.

Paul Harvey is a Senior Mechanical Design Engineer at Protean Electric. He holds a degree in Design and Innovation from the University of Portsmouth and has been specialising in advanced in-wheel motor concepts at Protean Electric (formerly PML Flightlink) since 2007.